Lestinen, Sami; Kilpeläinen, Simo; Kosonen, Risto; Jokisalo, Juha; Koskela, Hannu; Li, Angui; Cao, Guangyu

Indoor airflow interactions with symmetrical and asymmetrical heat load distributions under diffuse ceiling ventilation

Published in:
Science and Technology for the Built Environment

DOI:
10.1080/23744731.2019.1588029

Published: 03/07/2019

Document Version
Peer-reviewed accepted author manuscript, also known as Final accepted manuscript or Post-print

Indoor airflow interactions with symmetric and asymmetric heat load distributions under diffuse ceiling ventilation

SAMI LESTINEN[1,*], SIMO KILPELÄINEN[1], RISTO KOSONEN[1,2], JUHA JOKISALO[1], HANNU KOSKELA[3], ANGUI LI[4], GUANGYU CAO[5]

[1]*Aalto University, School of Engineering, Department of Mechanical Engineering, Sähkömiehentie 4, 02150 Espoo, Finland*
[2]*College of Urban Construction, Nanjing Tech University, China*
[3]*Turku University of Applied Sciences, Lemminkäisenkatu 14-18 B, FI-20520 Turku, Finland*
[4]*Xi'an University of Architecture and Technology, No. 13 Yanta Road, Xi'an, Shaanxi Province, P.R. China*
[5]*Norwegian University of Science and Technology, Department of Energy and Process Engineering, Kolbjørn Hejes vei 1b, 7491 Trondheim, Norway*
**corresponding author: sami.lestinen@aalto.fi*

Abstract

Heat load distribution and supply air jets affect considerably indoor airflow patterns which may cause local thermal discomfort. In this study, heat load distribution was studied at the heat load strength of 40 W/floor-m^2 and 80 W/floor-m^2 with diffuse ceiling ventilation. Experimental measurements were carried out in a test chamber of 5.5 x 3.8 x 3.2 m^3 by using omnidirectional anemometers and long averaging time. Indoor air temperature of test chamber was 26±0.5°C. In symmetric setup, cylindrical heat sources were located evenly on the floor. In asymmetric setup, two workstations were located near windows. This study recommends to reduce buoyancy and momentum driven flows in the occupied zone. In symmetric setup, the local draught rate exceeded 10% at least in one height at all the measured locations and heat load strengths in the occupied zone. In asymmetric setup, 47% of measured locations exceeded 10% at 40 W/floor-m^2 and 87% at 80 W/floor-m^2, correspondingly. Thus, thermal environment was classified as category B for 40 W/floor-m^2 and category C for 80 W/floor-m^2 according to EN ISO 7730 standard. Spatial differences increased with asymmetric setup compared to symmetric one, and those differences increased with heat load.

Keywords: office environment, heat load, thermal discomfort, draught, air velocity, diffuse ceiling ventilation

Introduction

Draught has been one of the largest thermal problem in modern offices. This is because low air speeds are difficult to achieve under the ventilation jets and the buoyancy driven flows from heat sources and heat sinks (Melikov et al., 2005; Kosonen et al. 2011, Koskela et al., 2012; Müller et al., 2013). This can be associated with understanding of different elements and their interaction which have shown to have a considerable effect on healthy indoor environments (Wierzbicka et al., 2018). Generally, the draught has been defined as an unwanted local convective cooling of a person (Fanger, 1970). Furthermore, high turbulence may cause discomfort due to fluctuation which enhance heat transfer (Fanger and Pedersen, 1977; Fanger et al., 1988; Melikov et al., 1997). In addition, cold vertical surfaces can provide downdraught to occupants (Heiselberg, 1994; Larsson and Moshfegh, 2002). Consequently, local thermal discomfort is usually caused by draught, high vertical air temperature difference, warm or cool surfaces as well as thermal radiation asymmetry (Olesen, 2000). Actually, the airflow direction affects significantly on draught perception (Mayer and Schwab, 1988). For instance, the rising natural convection flow may interact with the vertical supply airflow and reduce the convective cooling of skin (Toftum et al., 1997). The ventilation and air conditioning is necessary for bringing fresh air to occupants and removing heated air and pollutants from the breathing zone. However, heat loads and increased airflow rates may yield to a higher air speed levels and deviation, which increase draught discomfort (Müller et al., 2013). Therefore, it is not a surprise that draught has been a common complaint indoors (Hanzawa et al., 1987; Kosonen et al., 2011; Sakellaris et al., 2016). However, the ventilation requirements can be too low to prevent health and comfort problems (Seppänen et al. 1999; Wargocki et al., 2002; Seppänen and Fisk, 2004). Consequently, new framework for ventilation requirements has been proposed (Carrer et al., 2018). Generally, the acceptable thermal environments have been described in the ASHRAE standards and in the European ISO standards (ASHRAE, 2017; CEN, 2005; CEN, 2007).

A reasonable amount of clean air must be provided for indoor occupants. Furthermore, the raised temperatures may create a negative effect on health and performance (Wargocki and Wyon, 2007; Lan et al., 2011; Cao and Deng, 2019). Consequently, air distribution is one of the major factors for health, comfort and performance. A risk of draught increases when the airflow temperature decreases and the mean air velocity and turbulence intensity increase. On the contrary, the office-workers may require air movement at higher air temperature conditions. An earlier study shows that humans do not feel draught even at the air velocities of 0.4 m/s if the air temperature is above 23°C (Toftum, 2004). This indicates that air speed can be perceived comfortable at warm indoor conditions. One of the advantages in personalized ventilation systems is a user-control while compared to common mechanical ventilation systems (Melikov, 2004). The user-control is necessary, because a satisfaction with thermal environment is an individual feeling that is affected locally by the natural and forced convection as well as the thermal radiation asymmetry.

The indoor airflow pattern depends on the relative locations of air distribution units and heat sources (Koskela et al., 2010; Kosonen et al., 2010; Müller et al., 2013; Petersen et al., 2014). Therefore, different heat load distributions are recommended to be evaluated while designing thermal environments (Nielsen, 2007; Shao et al., 2018; Yin et al., 2019). When a low-momentum ventilation is used, the buoyancy flows drive the indoor air movement (Hagström et al., 2000; Nielsen et al., 2017). Generally, the human perception of air movement may depend on the air speed, air speed fluctuations, air temperature, and personal factors such as overall thermal sensation and activity level. In indoor climate, the kinetic energy will increase due to buoyancy flows and ventilation jets. Consequently, the local mean air speeds and deviation will increase (Hanzawa et al., 1987; Melikov et al., 1988; Hagström, 2002; Lestinen et al., 2018a). The indoor air velocity has been found to fluctuate from a very low level up to 2 Hz frequency (Finkelstein et al., 1996). The indoor airflows vary at different locations and heights and can be in a transitional state between the laminar and turbulent flow conditions (Heiselberg and Nielsen, 1996; Cheong et al., 2007; Kandzia and Müller, 2016). This means that the draught risk may rise even if the ventilation system provides locally a low-momentum supply airflow. In addition, earlier studies have emphasized the effects of heat load distribution on indoor airflows (Cho and Awbi, 2007; Koskela et al., 2012; Zhang et al., 2016; Nielsen et al., 2017). It follows that asymmetric heat load creates often a large-scale airflow pattern from heat sources to opposite side of room (Koskela et al., 2010; Bertheussen et al., 2013; Lestinen et al. 2018b). This large-scale airflow pattern circulates and can increase air speed levels particularly at the ankle height that, in turn, has been shown to increase a percentage of dissatisfied with draught (Liu et al., 2017).

Diffuse ceiling ventilation is a vertical air distribution system, in which an even supply of perforated suspended ceiling penetrates fresh air down to the occupied zone (Zhang et al., 2014). In principle, the diffuse ceiling ventilation may handle relatively large internal heat loads and improve thermal comfort (Jacobs et al. 2008; Jacobs and Knoll, 2009; Fan et al., 2013). The diffuse ceiling ventilation differs from a common piston ventilation such as the total supply opening area is much smaller than with the piston flow, and therefore, the air change rates can be reduced significantly (Cao et al., 2014). Furthermore, the diffuse ceiling may act as a radiant cooling that can increase a cooling potential (Hviid and Svendsen, 2013). However, the most probable draught risk comes from convection flows from heat sources (Nielsen, 2011). When the ventilation rate is increased, the local effects on indoor airflow conditions will be smaller under the diffuse ceiling ventilation than those with the traditional mixing ventilation or displacement ventilation systems. This is because a supply inlet area is often larger in the diffuse ceiling ventilation than in those other air distribution methods. For instance, a recent study shows that the mixing ventilation cannot provide a same cooling capacity without draught risk than the diffuse ceiling ventilation (Zukowska-Tejsen et al., 2016). Therefore, the diffuse ceiling ventilation can be a reasonable choice for open plan offices. However, recent studies have proposed that a combination of convective and radiant systems, e.g. a chilled-ceiling system, may decrease draught discomfort (Mustakallio et al., 2016; Mustakallio et al., 2017). In addition, a suggestive evidence has been found that the radiant system may provide equal or better thermal comfort than the convective systems (Karmann et al., 2017).

In this study, the motivation was to improve knowledge on airflow interactions and indoor air movement under diffuse ceiling ventilation system with differrent heat load conditions. The air change efficiency was measured as 40-50% in which nearly fully mixed conditions was obtained. Furthermore, the interaction of air jets and thermal plumes was investigated. This is because new knowledge on indoor airflow interactions are necessary for developing indoor environments in the future, in which the smart HVAC systems monitor and control indoor climate such as a thermal environment is optimal and acceptable. The main objective was to investigate the effects of heat load strength and heat load distribution on airflow interactions in the the occupied zone. The study contributes to indoor airflow technologies and human impacts on thermal environment. New knowledge are provided by conducting measurements and analysis in the controlled and simplified indoor environment. Moreover, the study improves understanding on indoor airflows, air velocity conditions and draught discomfort.

The novelty of this study lies on quantifying indoor airflow interactions under both the symmetric and asymmetric conditions of heat load distributions. The study investigates also a peak heat load conditions by using a long averaging time (h) and high sampling rate (Hz) that increase a reliability of measured dataset records in the descriptive statistics. New contribution can be also related to the interaction of buoyancy flows and equal low-momentum air distribution method, in which the horizontal and vertical flow profiles were explored. Consequently, a systematic investigation of time and spatial averaged airflow field was carried out in a controlled thermal environment such as the additional effective parameters were excluded. Furthermore, the descriptive statistical analysis was made to discover spatial and temporal deviation of flow field that indicated indoor air fluctuation and gradients in the thermal environment. Moreover, the given results can be further utilized in validating CFD simulation models. Additionally, the acceptance of thermal environment is discussed based on EN ISO 7730 draught rate model and how the heat load distribution may affect the level of category. When understanding better the airflow interaction, the healthy and comfortable indoor environments can be optimized more reliably than earlier by using the advanced and smart HVAC-technology. Thus, assessing airflow interactions is an essential part of human well-being indoors.

Methods

Test chamber

The test chamber (Figure 1) was located inside a laboratory hall in which the environment was stable. The test chamber internal dimensions were 5.5 m length, 3.8 m width and 3.2 m height. Above the suspended ceiling (Figure 1a) was an upper plenum chamber of 0.35 m for the duct diffuser of supplied fresh air. The diameter of duct diffuser was 0.2 m and the supply airflow pattern was 180° upwards. The suspended ceiling was made of glass wool elements. The measured perforation rate was 0.50±0.02 % and the nozzle diameter was 14 mm.

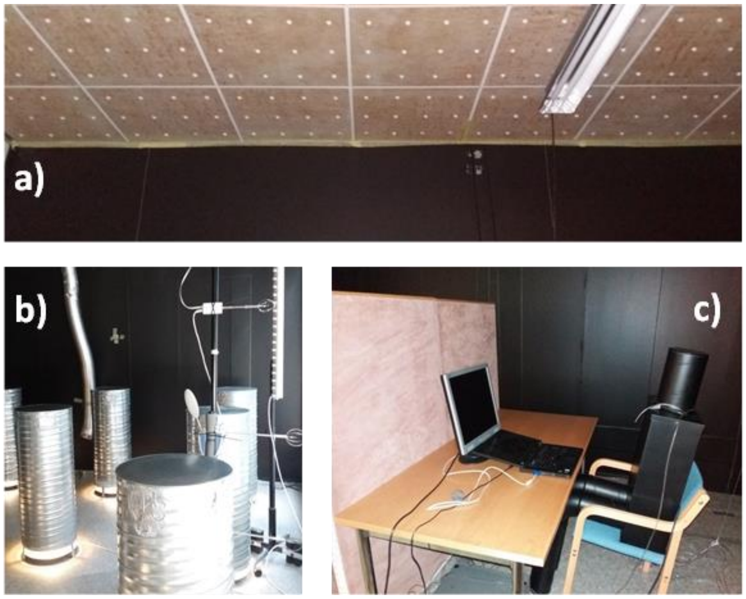

Figure 1. Test chamber: a) The diffuse ceiling inlet with a perforation rate of 0.50±0.02 %. b) The symmetric setup. c) The asymmetric setup.

Experimental set-up

The symmetric and asymmetric heat load distributions were compared. The heat load strength was 40 W/floor-m^2 and 80 W/floor-m^2 that describes the growth from a common heat load level up to a peak load level. The total heat load was adjusted to cover the set heat load. Thus, each heat source was measured and adjusted to respond the desired set of heat load. Furthermore, the ventilative cooling power was measured and adjusted to maintain the target room air temperature level. The indoor air temperature difference was kept at 9°C between the supply air and exhaust air by controlling the ventilation rate and supply air temperature. The supply air temperature was chosen as 17°C, because the cooler air is usually supplied into the room at the temperature level of 10°C below the room air temperature while all-air conditioning system is used. The exhaust air temperature was chosen as 26°C to characterize typical summer conditions. Table 1 summarizes the parameters of those setups.

Table 1. Parameters for the symmetric and asymmetric heat load setups (±accuracy). ACH is the air change rate.

Test cases	Case 40 W/floor-m^2	Case 80 W/floor-m^2
Floor area [m^2]	21±0.3	21±0.3
Heat load [W/floor-m^2]	40±2	80±4
Exhaust air temperature [°C]	26±0.5	26±0.5
Supply air temperature [°C]	17±0.1	17±0.1
Supply airflow rate [l/s,floor-m^2]	3.6±0.2	7.3±0.4

ACH [1/h]	4.0±0.3	8.2±0.6

The symmetric set-up consisted of 12 cylindrical heat sources with a diameter of 0.4 m and a height of 1.1 m (Figure 2a and Figure 2c). Each cylinder had two light bulbs and same setting for the heat power. The asymmetric set-up consisted of a double office layout (Figure 2b and Figure 2d). The workstations contained the seated dummy (88±5 W), laptop (48±3 W) and monitor (35±2 W). The workstations were located 0.6 m from the heated window panels (Figure 2b). Light (116±6 W) was installed at the suspended ceiling in the middle of the workstations (Figure 1c). Heating foil (420±21 W, 5x1 m^2, length x width) was installed on the floor 0.8 m from the parallel window wall to simulate direct solar radiation. The power of heating foil was measured and adjusted to respond the desired heat load. At the peak load conditions, a cubic heat source of 0.4x0.4x0.4 m^3 (103±5 W) was located under the table (Figure 2b, rectangle at the location 13). The dimensions of each window panel were 0.60 m width and 1.79 m height. A surface temperature setting of the window panels were adjusted to 30-40°C so that the target heat load level was achieved in the test chamber. In the symmetric heat load set-up, the indoor air was extracted from the height of 0.4 m above the floor (Figure 2a). In the asymmetric set-up, the indoor air was extracted at the suspended ceiling to follow a common design practices in office environments (Figure 2d). In the symmetric setup, the airflow field was rather similar in the different parts of test chamber. Consequently, the measured positions were located more densely than in the asymmetric heat load setup, in which the considerable differences were obtained between the different sides of the room. The detailed heat sources of the asymmetric setup are summarized in Table 2. Furthermore, Table 3 shows the boundary conditions of the measurements.

Table 2. Heat loads in the asymmetric set-up (±accuracy).

Test case	40 W/m^2	80 W/m^2
2 x dummy [W]	176±9	176±9
2 x laptop [W]	96±5	96±5
2 x monitor [W]	70±4	70±4
Cube load at floor [W]	0	103±5
Light [W]	116±6	116±6
7 x window panel [W]	381±19	696±35
Heat load at floor [W]	0	420±21
Total heat load [W]	839±42	1677±84

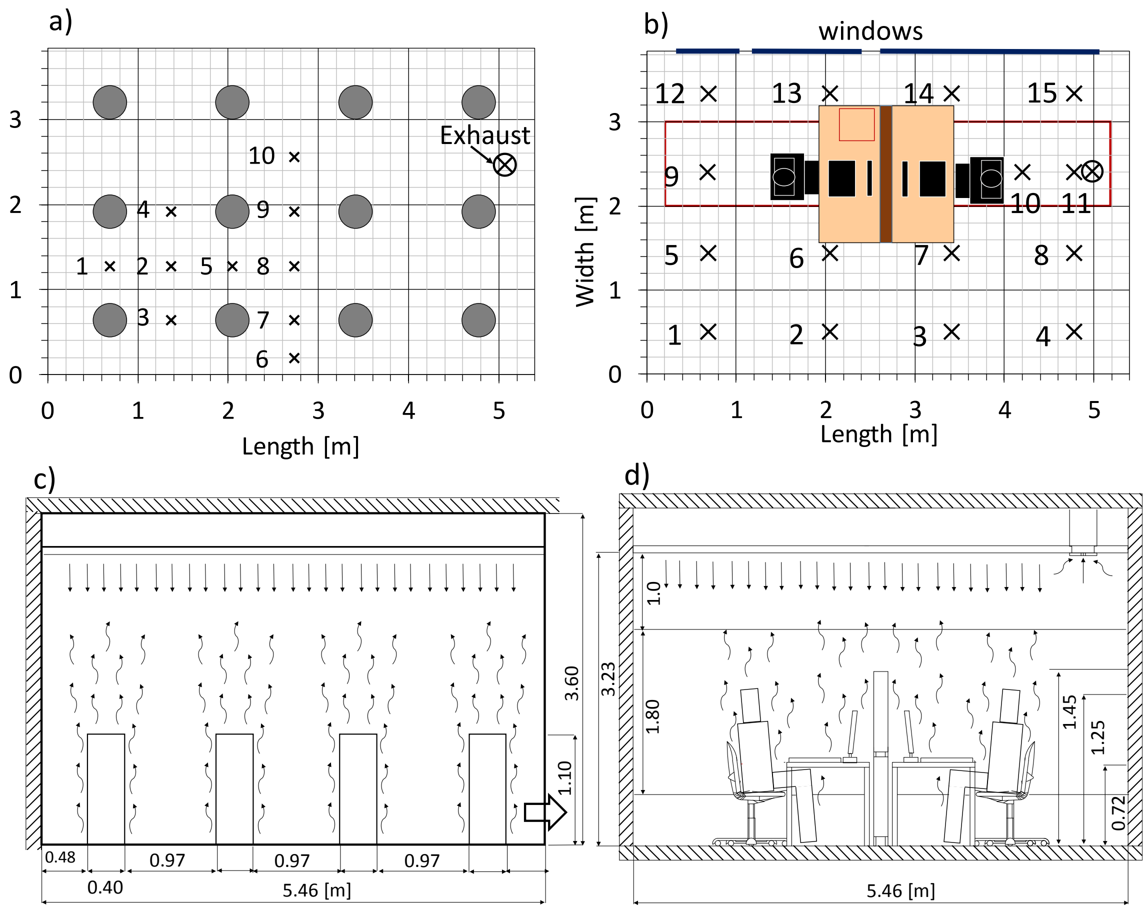

Figure 2. The measurement locations (x) and the heat load distribution: a) The symmetric heat load setup with the cylindrical heat sources. b) The asymmetric heat load setup with the workstations and windows. c) Side-view of the symmetric setup. d) Side-view of the asymmetric setup.

Table 3. Average boundary conditions at surfaces (±accuracy).

Test case	Symmetric	Symmetric	Asymmetric	Asymmetric
Heat load strength	40 W/fl-m^2	80 W/fl-m^2	40 W/fl-m^2	80 W/fl-m^2
Floor layer air temperature (offset 1.5 cm)	25±1°C	25±1°C	25±1°C	26±1°C
Wall layer air temperature, (offset 2 cm)	25±1°C	26±1°C	25±1°C	26±1°C
Window panel wall air temp (offset 2 cm)	25±1°C	25±1°C	28±1°C	30±1°C
Cylindrical dummy, chest temperature	32±2°C	38±2°C	-	-
Seated dummy, chest temperature	-	-	36±2°C	36±2°C
Window panel temperature	25±2°C	26±2°C	33±2°C	39±2°C

Measuring instruments

The anemometers (Table 4) were installed at heights 0.1 m, 0.6 m, 1.1 m, 1.4 m, 1.7 m, 2.3 m and 2.9 m according to recommendation by the standard EN ISO 7726 (CEN, 2001). In the symmetric set-up, the sampling rate was 1 Hz in the lower zone from 0.1 m up to 1.1 m, and 0.5 Hz in the upper zone from 1.4 m up to 2.9 m, because the main frequency level for human discomfort due to air velocity has been found to be around 0.3-0.5 Hz (Fanger and Pedersen, 1977). The measuring interval was 0.5 h. In the asymmetric set-up, the sampling rate was increased up to 10 Hz in the seated person zone to detect wider range of frequencies. The sampling rate was kept at 0.5 Hz in the upper zone. The measuring interval was 1 h. The dynamic response time for the air temperature was below 1 s in the seated person zone.

Table 4. Measuring instruments.

Meter type	Variable	Accuracy
Omnidirectional anemometer	Air temperature Air speed (at height 0.1 m-1.1 m)	Air speed: ±0.01 m/s ±2.5% of reading Air temperature: ±0.15°C Sampling rate 10 Hz STDerr < 10 % up to 2 Hz time-constant < 1 s (temperature)
Omnidirectional anemometer	Air temperature Air speed (at height 1.4 m-2.9 m)	Air speed: ±0.02 m/s ±1.5% of reading Air temperature: ±0.2°C Sampling rate 8 Hz STDerr < 10% up to 1.5 Hz
Tinytag data logger	Air temperature	±0.5°C (0…+45°C)
Infrared camera	Surface temperature	±2°C or ±2% of reading
Infrared thermometer	Surface temperature	±1°C or ±1% of reading
Measuring instrument	Pressure difference	±0.3% of reading, lowest ±0.3Pa
Regulation and measuring device	Airflow rate	±5%

Airflow characteristics

The instantaneous air speed in the measured time series records can be divided into a time-averaged component and a fluctuating component as

$$U(x,y,z,t) = \overline{U}(x,y,z) + U'(x,y,z,t)\,, \tag{1}$$

where U [m/s] is the instantaneous air speed in the discrete data set, x, y, z [m] refers to the length, width and height coordinates at the measured location, t [s] is the time, $\overline{U}$ [m/s] is the time-averaged component of air speed and U' [m/s] is the instantaneous fluctuating component of air speed. The time-averaged component is expressed by

$$\overline{U}(x,y,z) = \frac{1}{T}\sum_{n=1}^{T} U(x,y,z,t)_n \Delta t_n\,, \tag{2}$$

where T [s] is the time interval of measurements in the discrete dataset records, Δt [s] is the time-step size between the readings and subscript n denotes the index notation for the discrete values. The sample standard deviation is written correspondingly

$$U_{std} = \sqrt{\frac{\sum_N \left(U_i - \overline{U} \right)^2}{N-1}}\,. \tag{3}$$

The local draught rate model of EN ISO 7730 standard is defined as

$$DR(x,y,z) = (34 - t)(\overline{U} - 0.05)^{0.62}(0.37 \cdot \overline{U} \cdot Tu + 3.14)\,, \tag{4}$$

in which t [°C] is the local air temperature from 20°C to 26°C, $\overline{U}$ [m/s] is the local mean air speed from 0.05 m/s to 0.5 m/s, and Tu [%] is the local turbulence intensity from 10 % to 60 %. The model is applicable to people at light activity, e.g. to a sedentary person. However, the model may overestimate the predicted draught rate at the arms and feet levels. The turbulence intensity is expressed as

$$Tu(x,y,z) = \frac{U_{std}(x,y,z)}{\overline{U}(x,y,z)} \times 100\ [\%]\,. \tag{5}$$

The normalized air temperature is expressed as

$$T_n = \frac{\bar{T} - \bar{T}_{in}}{\bar{T}_{out} - \bar{T}_{in}} \, , \tag{6}$$

where $\bar{T}$ [°C] is the local mean air temperature. The seated person zone is defined as an indoor air volume below the height of 1.2 m. The occupied zone is defined correspondingly below the height of 1.8 m. Hence, the seated person zone included the anemometer positions of 0.1 m, 0.6 m and 1.1 m. The occupied zone included the heights of 0.1 m, 0.6 m, 1.1 m, 1.4 m and 1.7 m. In the symmetric setup, the corridor side was the locations 3 and 7. The middle of the room was locations 4 and 9 (Figure 2a). In the asymmetric setup, the corridor side was locations 1-4, the middle of the room was locations 5-8 and the window side was locations 12-15 (Figure 2b).

Results

Air temperature

The air temperatures were at the same level in the room side and in the middle of the room while the symmetric setup was investigated (Figure 3a and Figure 4a). In contrast, the average of local mean air temperatures was different between the middle of the room and the room sides when the asymmetric setup was observed (Figure 3b and Figure 4b). This was the main effect while changing the heat load distribution. In double office layout, the air temperature was highest in the window side and lowest in the corridor side, because the heat loads were in the perimeter area. However, both of those heat load distributions provided the thermal conditions, in which the spatial average of mean air temperatures increased from the ankle height up to the head height of seated person. Furthermore, the air temperature decreased from the head height up to the ceiling zone due to colder supply air. This may characterize a vertical air temperature profile in an office environments with diffuse ceiling ventilation. In the symmetric setup, the vertical mean air temperature gradients were below 0.9°C/m in the occupied zone. In the asymmetric setup, the corresponding vertical gradients were smaller, below 0.5°C/m. The vertical air temperature difference was within a degree, thus the averaged effect on human thermal discomfort can be assumed small (ISO 7730).

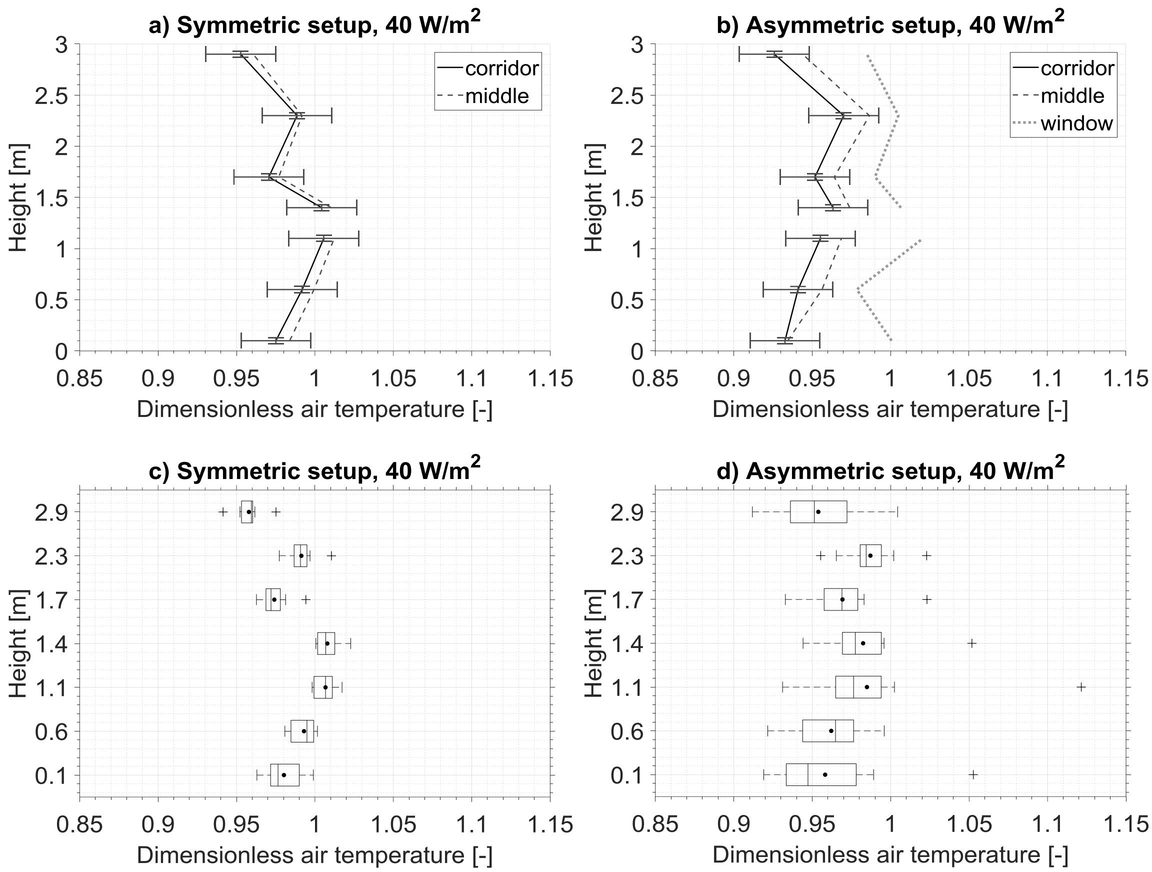

Figure 3. Dimensionless air temperature as a function of room height at 40 W/floor-m^2: a) Symmetric setup. b) Asymmetric setup. The horizontal and vertical error bars indicate the uncertainty in measurement. c) Boxplot of symmetric setup. d) Boxplot of asymmetric setup. The box indicates the 25th percentile, median and 75th percentile of the dimensionless mean air temperatures of measured locations at a given height. The whiskers denote a range of those air temperatures and the outliers are plotted individually. The dot in the box refers to the mean of dataset.

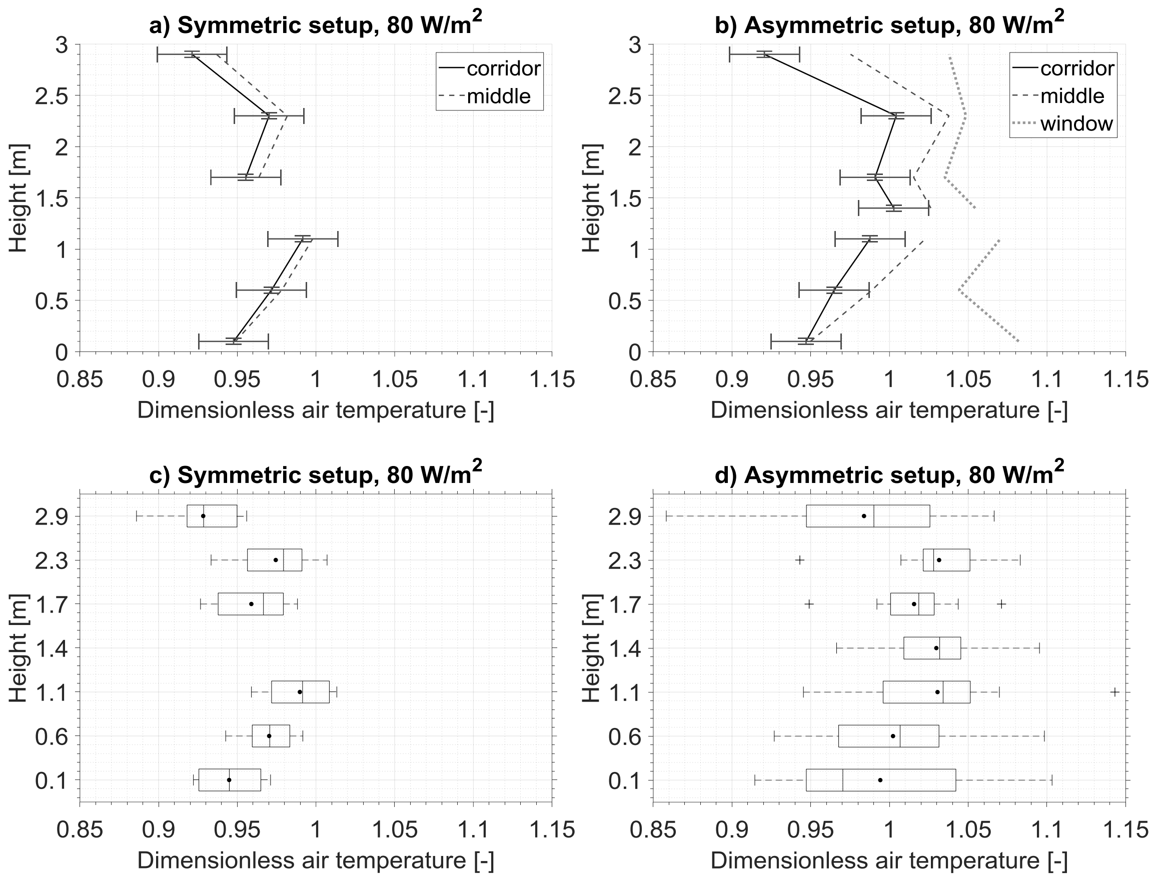

Figure 4. Dimensionless air temperature as a function of room height at 80 W/floor-m^2: a) Symmetric setup. b) Asymmetric setup. The horizontal and vertical error bars indicate the uncertainty in measurement. c) Boxplot of symmetric setup. d) Boxplot of asymmetric setup. The box indicates the 25th percentile, median and 75th percentile of the dimensionless mean air temperatures. The whiskers denote a range and the outliers are plotted individually. The dot in the box refers to the mean of dataset.

Consequently, the asymmetric heat load distribution provided a greater difference between the room sides than the symmetric one. Furthermore, this difference increased with heat load. This means that an attention should be given to the heat load management with higher internal heat load levels. In addition, the marker smoke visualizations showed that the asymmetric setup generated a large-scale circulating airflow pattern from the window side to the opposite corridor side along to ceiling zone. The airflow pattern returned to the workstations along to floor zone across the room. However, this airflow can not be warm air, since the warm air stays at the ceiling zone until cooled or extracted. Furthermore, the air temperature was lower in the corridor side, because the supply air was turned sidewise down to the corridor volume due to the buoyancy driven flows from perimeter area. This circulating airflow pattern was not found with the symmetric setup.

In the symmetric and asymmetric setups, both the temporal standard deviation of air temperatures and the spatial standard deviation of local mean air temperatures increased with the heat load strength. However, the spatial deviation was greater than the temporal deviation (Figure 5). Furthermore, the temporal deviation was lower, but the spatial deviation was higher with the asymmetric setup than with the symmetric one. Consequently, the results imply rather small temporal deviation with diffuse ceiling ventilation at the peak heat load conditions, indicating a stable airflow field in the room. Hence, a larger average difference occurs spatially between the measured locations than that of temporally in the airflow field. However, the average deviation dampen the local fluctuations that may have considerable effects on sensation with thermal environment at the workstations.

Figure 5 shows the spatial and temporal deviations of air temperature at the ankle height and at the head height of seated person at 80 W/floor-m^2. Those heights are essential when estimating a sensation of draught. In the symmetric setup, the temporal deviation was slightly higher at the head height than at the ankle height. In the asymmetric setup, the difference between the room sides was significant. This statistics supplement the average result that temporal deviation was smaller in the asymmetric setup than in the symmetric one.

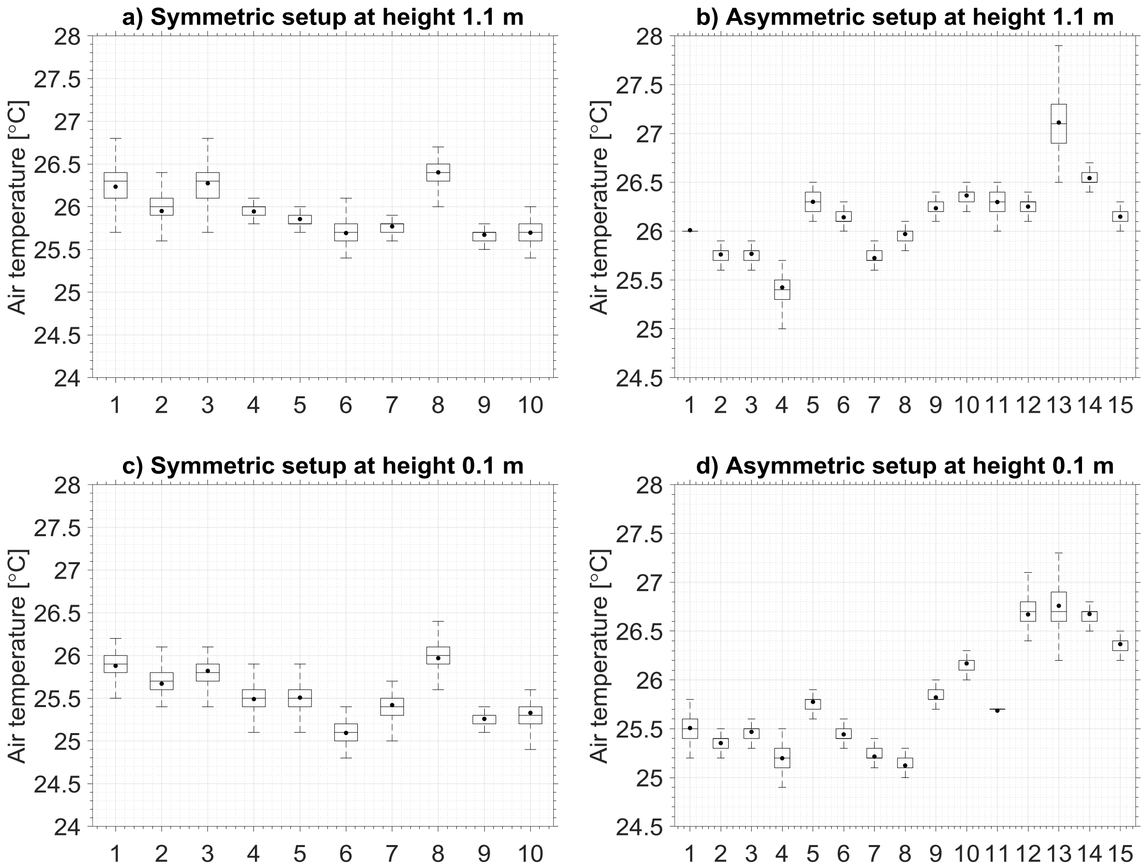

Figure 5. Spatial and temporal statistics of air temperature at 80 W/floor-m^2 in the seated person zone: a) Symmetric setup at the head height. b) Asymmetric setup at the head height. c) Symmetric setup at the ankle height. d) Asymmetric setup at the ankle height. The x-axis denotes the measuring locations (Figure 2). The box indicates the 25th percentile, median and 75th percentile of instantaneous air temperatures at a given location. The whiskers denote a range of those air temperatures excluding outliers. The dot in the box refers to the mean of dataset.

Air speed

Figure 6 and Figure 7 show the characterizing air speed profiles. In the symmetric setup, the average mean air speed decreased from the ankle height up to the head height of seated person and then remained rather similar up to the ceiling zone. In the asymmetric setup, the average mean air speed increased both at the floor and at the ceiling levels. Most probably, this is due to large-scale circulating airflow pattern, which increases the mean air speed levels also close to the ceiling zone. In both of those setups, approximately same amount of kinetic energy was released into the room. However, part of the kinetic energy entered to the circulating airflow pattern with the asymmetric heat load distribution. Therefore, the average mean air speed of seated person zone was slightly lower in the asymmetric setup than in the symmetric one. Furthermore, the relative difference between those setups increased with heat load.

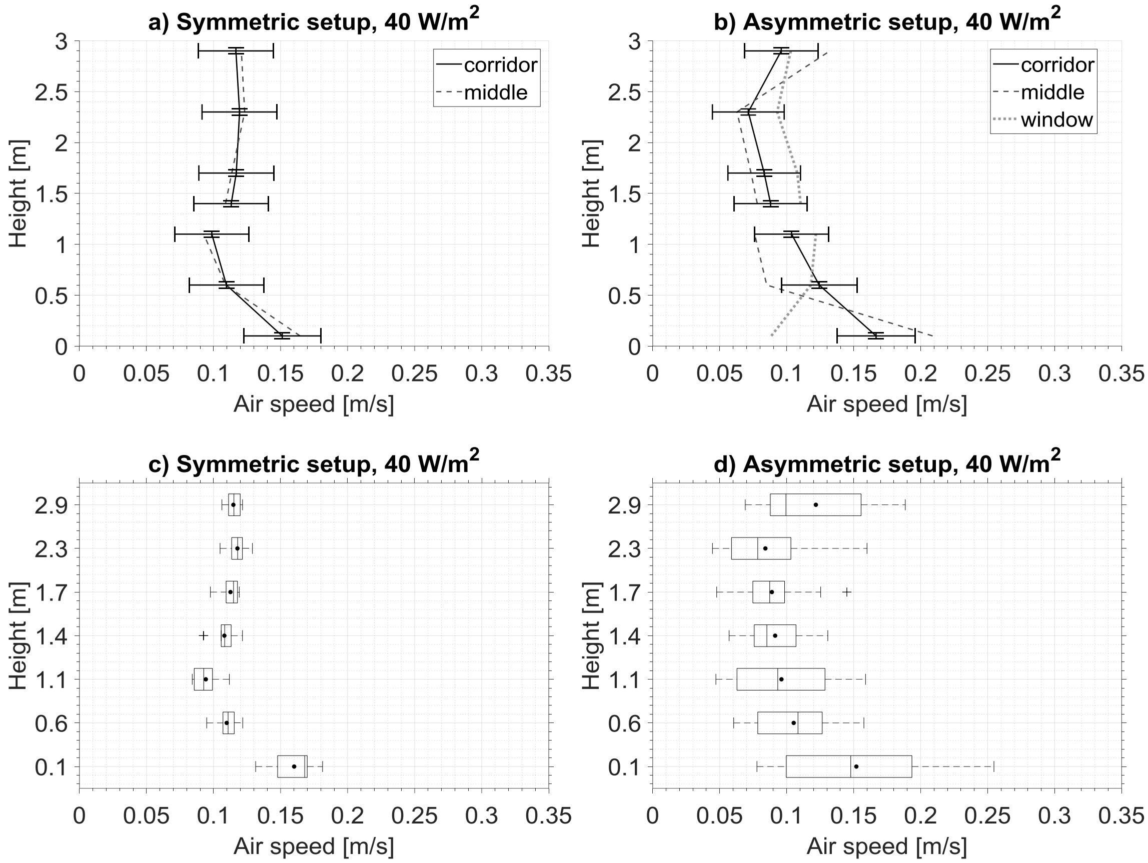

Figure 6. Air speed at 40 W/floor-m^2: a) Symmetric setup. b) Asymmetric setup. c) Boxplot of symmetric setup. d) Boxplot of asymmetric setup. The horizontal and vertical error bars indicate the uncertainty in measurement. The box indicates the 25th percentile, median and 75th percentile of the mean air speeds of measured locations at a given height. The whiskers denote a range of those air speeds and the outliers are plotted individually. The dot in the box refers to the mean of dataset.

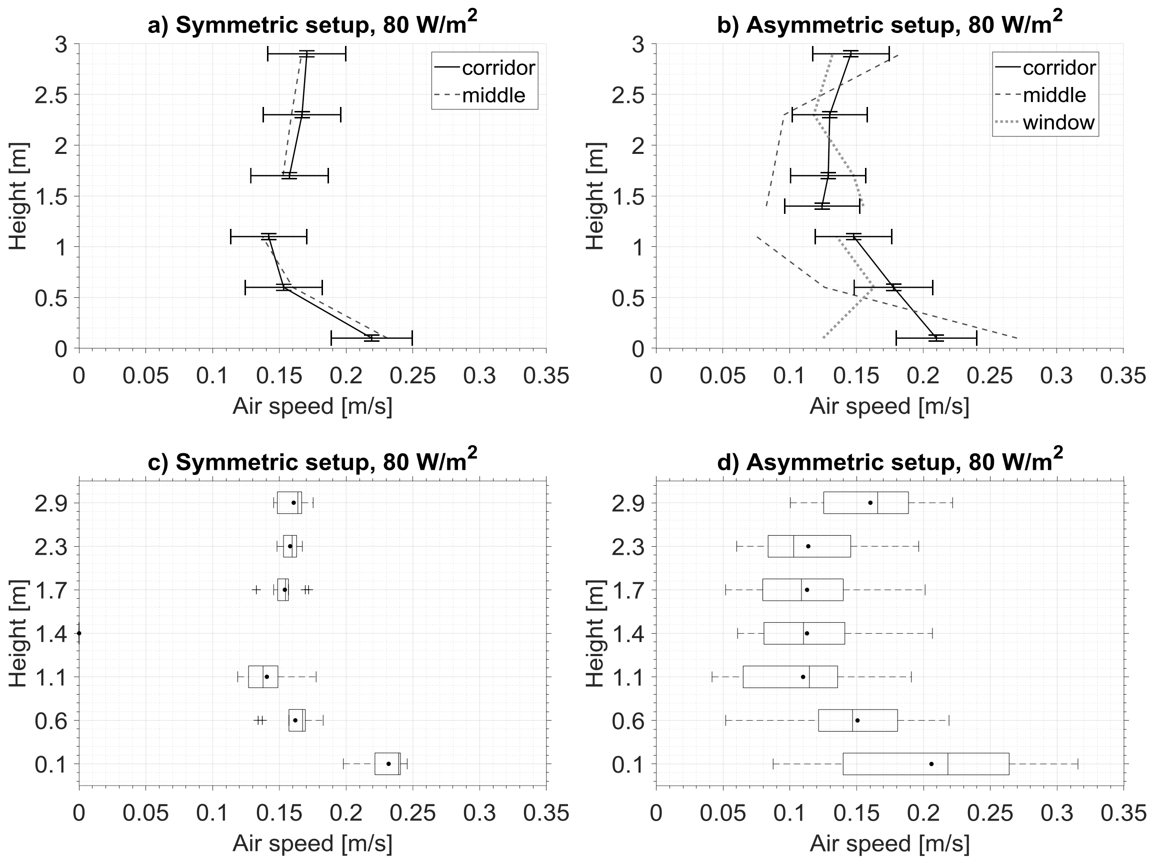

Figure 7. Air speed at 80 W/floor-m^2: a) Symmetric setup. b) Asymmetric setup. c) Boxplot of symmetric setup. d) Boxplot of asymmetric setup. The horizontal and vertical error bars indicate the uncertainty in measurement. The box indicates the 25th percentile, median and 75th percentile of the mean air speeds. The whiskers denote a range and the outliers are plotted individually. The dot in the box refers to the mean of dataset.

In the symmetric setup, the average of local mean air speeds was 0.12 m/s in the seated person zone both in the middle of the room and in the corridor side at 40 W/floor-m^2. The corresponding averages were 0.18 m/s and 0.17 m/s at 80 W/floor-m^2, respectively. In the asymmetric setup, the spatial air speed differences mainly increased compared to symmetric one, and those differences increased with heat load. Hence, the average air speed of the seated person zone was only 3.0 % lower in the asymmetric setup than in the symmetric setup at 40 W/floor-m^2. However, the corresponding relative difference increased up to 13 % at 80 W/floor-m^2. Thus, the average air speed was slightly higher with the equally located heat loads than with the perimeter area heat loads, and the relative difference between those setups increased at the peak load conditions.

On the contrary, the corresponding average of the corridor side was higher in the asymmetric setup than in the symmetric setup. Most probably, this is also due to circulating airflow pattern with the asymmetric setup, which increased the air speed levels locally and, as a consequence, increased the spatial differences compared to symmetric one. Therefore, in the asymmetric setup, the spatial standard deviation of local mean air speeds was significantly greater in the middle of the room than in the window side or in the corridor side. In the symmetric setup, the corresponding spatial deviation was more near each other in the measured locations.

In the testchamber, the air speed levels were higher at 80 W/floor-m^2 than at 40 W/floor-m^2, similar to that of the symmetric setup. However, the maximum mean air speed was higher in the asymmetric setup than in the symmetric one both in the corridor side and in the middle of the room. In the asymmetric setup, the vertical mean air speed gradients were greater in the middle than on the window side or on the corridor side, in contrast to that obtained for the symmetric setup where the gradients were more similar. Furthermore, the gradients increased with increasing of heat load. Therefore, the highest and the lowest mean air speed levels were found in the middle of the room with the asymmetric setup.

In the symmetric setup, the temporal deviation was greater than the spatial deviation, in contrast to that observed for the air temperature. Figure 8 shows the differences in spatial and temporal deviations between the head height and the ankle height of the seated person. The results shed light on airflow fluctuation in both the heat load setups. The results show that the air speeds were more equal in the symmetric setup than in the asymmetric setup, because the heat load of symmetric setup was equally distributed on the floor.

The experiments show that the average of mean air speeds, the spatial deviation of mean air speeds and the temporal deviation of instantaneous air speeds increased with heat load in both the symmetric and asymmetric heat load distributions. Consequently, also the range and maximum of air speeds increased. The temporal deviation of air speeds was higher in the symmetric setup than in the asymmetric setup. However, the spatial deviation of mean air speeds was smaller in the symmetric setup than in the asymmetric one. Thereby, the experiments reveal greater spatial gradients of the mean air speed with the asymmetric setup than with the symmetric one, although the temporal air speed deviation was larger.

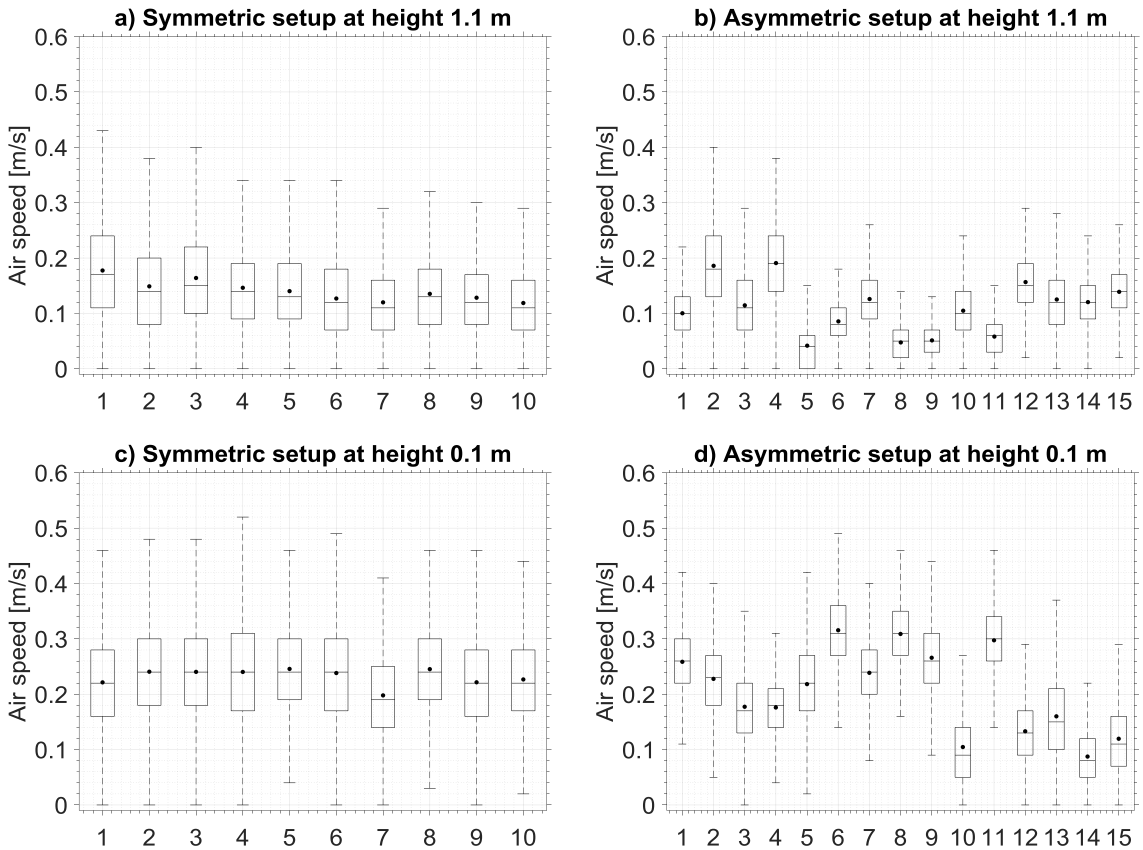

Figure 8. Spatial and temporal statistics of air speed in the seated person zone at 80 W/floor-m^2: a) Symmetric setup at the head height. b) Asymmetric setup at the head height. c) Symmetric setup at the ankle height. d) Asymmetric setup at the ankle height. The box indicates the 25th percentile, median and 75th percentile of instantaneous air speeds at a given location. The whiskers denote a range of air speeds excluding the outliers. The x-axis denotes the measuring locations (Figure 2). The dot in the box refers to the mean of dataset.

Turbulence intensity

The heat load had only a small effect on the average turbulence intensity in both setups, because both the temporal standard deviation of air speeds and the mean air speed increased with head load. However, the turbulence intensity mainly increased towards the decreased mean air speed levels, because the mean air speed decreased more than the temporal standard deviation of air speeds. Consequently, the lowest average intensity was obtained near the ankle height at 0.1 m and the highest average intensity near the head height of seated person at 1.1 m, in contrast to that obtained for the air speed conditions. This may increase heat transfer at the head level although the average air speed was low (Figure 9 and Figure 10).

In the symmetric setup, the local turbulence intensity ranged from 37 % to 65 % at 40 W/floor-m^2 (Figure 9c) and from 31 % to 59 % at 80 W/floor-m^2 (Figure 10c) in the seated person zone. Hence, those ranges were at the same level in the both heat load strengths. In the asymmetric setup, the local turbulence intensity ranged from 19 % to 85 % at 40 W/floor-m^2 (Figure 9d) and from 18 % to 84 % at 80 W/floor-m^2 (Figure 10d) in the seated person zone. Thus, those ranges were rather equal and also the average intensity was at the same level at both heat load strengths. However, those ranges were greater in the asymmetric setup than in the symmetric one. This follows closely the corresponding results in the mean air speed and in the deviation of air speeds such as the spatial differences increased with the asymmetric setup.

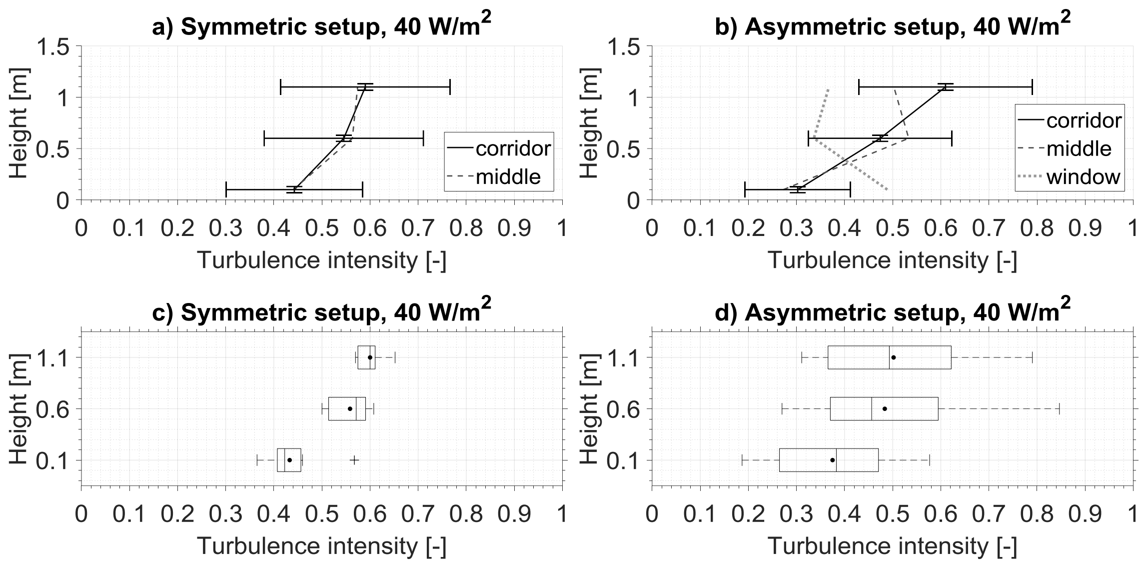

Figure 9. Turbulence intensity at 40 W/floor-m^2: a) Average turbulence intensity in the symmetric setup. b) Average turbulence intensity in the asymmetric setup. c) Boxplot of symmetric setup. d) Boxplot of asymmetric setup. The horizontal and vertical error bars indicate the uncertainty in measurement. The box indicates the 25th percentile, median and 75th percentile of the local turbulence intensities. The whiskers denote a range and the outliers are plotted individually. The dot in the box refers to the mean of dataset.

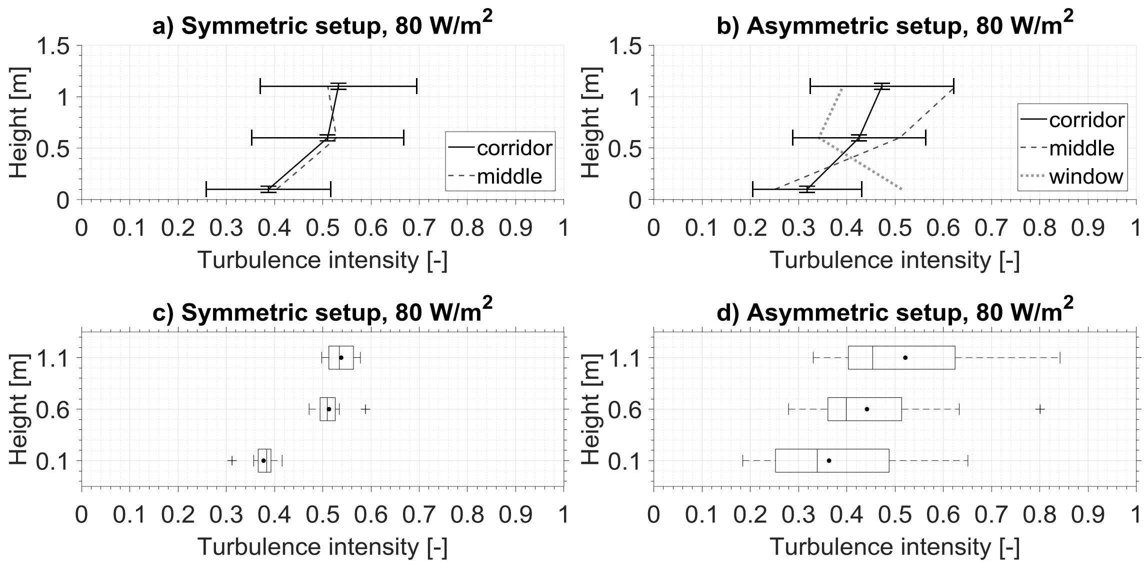

Figure 10. Turbulence intensity at 80 W/floor-m^2: a) Average turbulence intensity in the symmetric setup. b) Average turbulence intensity in the asymmetric setup. c) Boxplot of symmetric setup. d) Boxplot of asymmetric setup. The horizontal and vertical error bars indicate the uncertainty in measurement. The box indicates the 25th percentile, median and 75th percentile of the local turbulence intensities. The whiskers denote a range and the outliers are plotted individually. The dot in the box refers to the mean of dataset.

Draught rate

Figure 11 shows the maximum draught rate in the occupied zone at the given location. Generally, the draught rate increased mainly with the mean air speed level. In the symmetric setup, 22% of all the measured points exceeded the draught rate level of 10 % in the occupied zone at 40 W/floor-m^2. This share increased up to 85% at 80 W/floor-m^2. Hence, the evaluated draught discomfort increased with the combined effect of heat load and airflow rate. In the asymmetric setup, the corresponding shares were 12% and 35%, under 40 W/floor-m^2 and 80 W/floor-m^2 conditions, respectively. In the symmetric setup, the local draught rate exceeded 10% at least in one height at all the measured floor locations in the occupied zone at both heat load strengths. Thus, the share of floor locations was 100%, in which a risk of thermal discomfort was above 10% due to draught. This describes generally a thermal discomfort risk in the room, because even one location around a human body can worsen the thermal sensation to a non-acceptable level. However, the model may overestimate the predicted draught rate at the heights of 0.1 m and 0.6 m as defined by the ISO 7730 (CEN, 2005). In the asymmetric setup, 47% of floor locations exceeded 10% at 40 W/floor-m^2 and 87% of floor locations at 80 W/floor-m^2, correspondingly. Thus, those portions were smaller in the asymmetric setup than in the symmetric one. However, the maximum draught rate was at the same level in the both setups. This reveals that the draught discomfort was generally lower in the asymmetric setup than in the symmetric setup. Most probably, this is because part of the momentum goes to the large-scale circulation airflow in the asymmetric setup, which on the one hand, increase the spatial differences, and on the other hand, decrease the draught rate levels in the middle of the room air volume. Therefore, a share of locations was higher and more uniform with the symmetric setup than with the asymmetric setup.

In the symmetric setup, the maximum draught rates ranged from 11% to 15% under 40 W/floor-m^2 condition and from 16% to 21% under 80 W/floor-m^2 condition in the occupied zone below the height of 1.7 m. In the asymmetric setup, the maximum of local draught rates ranged from 6% to 18% at 40 W/floor-m^2, and from 9% to 21% at 80 W/floor-m^2 in the occupied zone. Consequently, those ranges were greater in the asymmetric setup than in the symmetric one, because asymmetry increased spatial differences in the airflow field. The largest vertical gradient of average draught rates was obtained in the middle of the room at the both head loads. With the both heat load distributions, a thermal environment would be classified as category B at 40 W/floor-m^2 and category C at 80 W/floor-m^2 according to EN ISO 7730 standard.

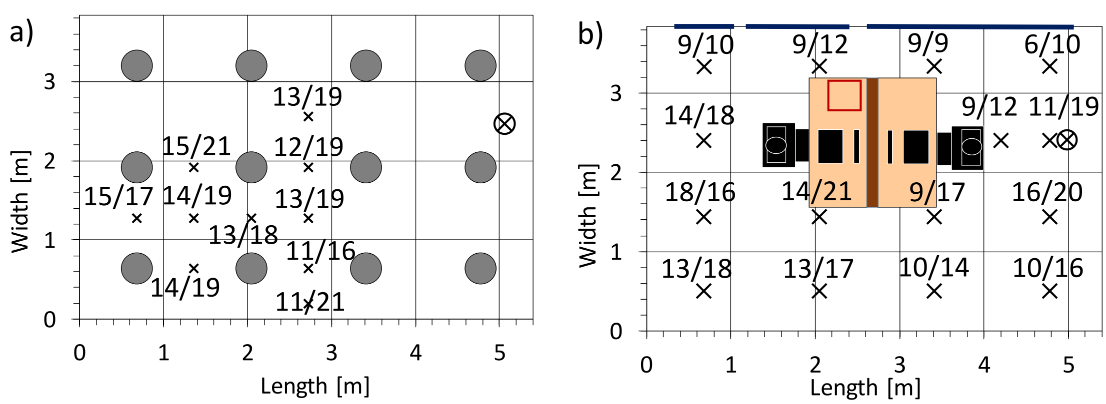

Figure 11. The maximum draught rate [%] in the occupied zone at 40 W/floor-m^2 and at 80 W/floor-m^2 marked as 40/80 at each floor location, respectively: a) Symmetric setup. b) Asymmetric setup. The category for thermal environment defined by EN ISO 7730: The category A (DR<10 %), category B (DR<20 %) and category C (DR<30 %).

The average draught rate and the deviation of draught rates increased with heat load in the both setups (Figure 12). This may characterize the change in draught discomfort towards increased heat load. However, the average draught rate was greater in the symmetric setup than in the asymmetric setup at the both heat loads. In addition, the spatial deviation was higher in the asymmetric setup than in the symmetric one. Figure 13 shows the linearized relationship of the air speed and the draught rate as a function of heat load strength in the seated person zone.

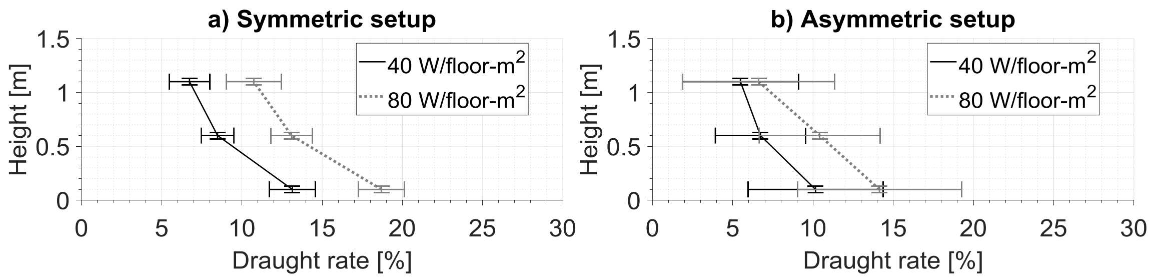

Figure 12. The average draught rate at 40 W/floor-m^2 and 80 W/floor-m^2 in the seated person zone: a) Symmetric setup, b) Asymmetric setup. The horizontal error bars indicate the standard deviation of local draught rates and the vertical error bars denote the uncertainty in height.

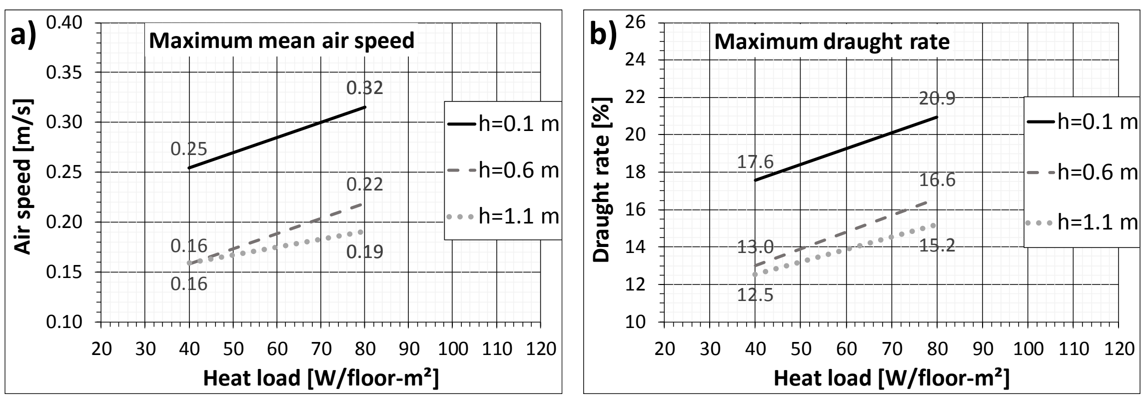

Figure 13. The air speed and the draught rate as a function of heat load strength at the heights of 0.1 m-1.1 m in the seated person zone on the asymmetric setup, i.e. the office layout: a) The maximum of mean air speeds b) The maximum draught rate. ACH from 4 to 8 (Table 1).

Discussion

The study indicates that it is difficult to achieve the category A of thermal environment stated in the EN ISO 7730 even at a common heat load conditions. The heat load distribution had a small effect on the classification, but the range of local maximums increased with the asymmetric setup compared to symmetric one. However, a reasonable uncertainty in measurement can be around 5 % p.p. (Melikov et al., 2007), thus the uncertainty in category exists correspondingly. Furthermore, the draught rate model may overestimate the predicted draught risk at heights 0.1 m and 0.6 m as stated in ISO 7730 (CEN, 2005). Generally, the highest draught rate was obtained at the ankle height and the lowest one at the head height of a seated person. Furthermore, the relative changes in draught rate seemed to follow rather closely the relative changes in mean air speed. The draught discomfort can be reduced by decreasing heat sources or by increasing water cooling power so that the required ventilation rate gets smaller. The results are valid only with the given experimental set-ups, and therefore, further studies are recommended with advanced cooling systems and heat load layouts. In the office setup, the short circuit of ceiling supply airflow can be avoided by extracting indoor air near the floor instead of ceiling. However, the warm air rises up to the ceiling zone. Therefore, the exhaust at the suspended ceiling can be also a reasonable choice in order to extract the heated flows.

The marker smoke visualization evidenced that the asymmetric heat load distribution generates a large-scale circulating airflow pattern from the heat sources to the other side of the room. This is because buoyancy forces accelerate the airflow upwards and turn the flow towards opposite corridor side along the ceiling. The return flow comes to the workstations along to floor that may increase a sensation of draught at the leg height of a seated person. Those findings agree with the earlier studies by Koskela et al. (2010) and Bertheussen et al. (2013). The satisfaction with thermal environment can be improved by using local adjustable ventilation and by preventing circulating airflow patterns on the floor, e.g. with the flow barriers and partition walls. Furthermore, the airflow patterns can be dampened at walls by internal architecture, such as green walls and curtains that may further enhance indoor environment while optimizing well-being and human health. The heat loads, which are concentrating in one region, can generate airflow patterns that circulate in the room and affect the air distribution flows. Consequently, air distribution should be designed such as the buoyancy flows from heat sources do not able to disturb the air distribution flows, e.g. ventilation jets. This ensures high performance of air distribution system. In addition, the human movement can have an effect on the airflow field at workstations.

In the symmetric setup, significant air temperature and air speed differences were not obtained between the corridor side and the middle of the room, because the heat loads were equally distributed on the floor. In the asymmetric setup, the average air temperature was slightly higher in the window side than in the opposite side, because the air was heated in the window side. Consequently, the supply air decreased the air temperature at a lower level in the corridor side. In contrast, the average air speed was higher in the corridor side than in the window side. However, the highest and the lowest mean air speed levels were found in the middle of the room.

The results show that the mean air speed and both the spatial and temporal deviations of air temperature and air speed increase with heat load. Therefore, also the draught rate will increase with the heat load. This is because the ventilation rate will increase when the heat load increases, thus the indoor airflow motions increase due to larger buoyancy flows and momentum flows that, in turn, interact with each other. The average air temperature increased from the ankle height up to the head height of seated person, and then decreased up to the ceiling zone due to supply air. This may characterize the vertical air temperature distribution with diffuse ceiling ventilation. In the symmetric setup, the average indoor air temperature was lower than the exhaust air temperature. Furthermore, the growth in the heat load increased the difference, in contrast to the asymmetric setup, in which the average indoor air temperature was greater than the exhaust air temperature at 80 W/floor-m^2. The reason for that is most probably a higher spatial deviation of air temperature in the asymmetric setup than in the symmetric one. In addition, the equally distributed heat load dampened the spatial deviation in the symmetric setup.

The management of indoor airflows is an important matter while decreasing a risk of draught. This means that a control of indoor airflows have to be performed case-dependently such that a smart control system can identify changes in indoor climate, and as a consequence, adjust new settings to maintain acceptable indoor conditions. Therefore, new type of monitoring system should be developed. The ventilation performance is highly affected by the heat loads, settings of HVAC systems and geometry of the enclosures. The future trends in airflow interaction may be assessed e.g. by conducting CFD simulation methods with the actual boundary conditions.

Overall, the airflow motions will increase with heat load and ventilation rate in indoor environments. This means that not only the spatial and temporal fluctuation will increase, but also gradients and range of scales will increase that interact with each other, which in turn can have an effect on satisfaction with thermal environment. Those parameters have not been taken completely account in the standards. Further improvements could be considered for thermal environment by directing buoyancy flows immediately into the exhaust at the ceiling zone or dampen the flows locally. In addition, properly designed advanced cooling systems may enable optimal thermal conditions and low draught such that airflow patterns are reasonable at workstations. Therefore, a common recommendation is either to decrease heat sources or implement user-centric ventilation systems involving radiative systems and personalized ventilation in the future indoor environments.

Conclusions

- With the diffuse ceiling ventilation system used in this study, thermal environment was classified as category B for 40 W/floor-m^2 and category C for 80 W/floor-m^2 in EN ISO 7730. Hence, category A was not obtained, although the low-momentum ventilation method was applied that covered equally the entire occupied zone. However, an uncertainty in measurement can be around 5% (p.p.) and the model may overestimate the predicted draught risk at the height of 0.1 m and 0.6 m in which the highest draught rates were found.
- The study recommends that the buoyancy and momentum driven flows should be reduced, removed or dampened in the occupied zone at increased heat load conditions. Otherwise, indoor airflows can be difficult to control at the workstations.
- The spatial differences increased with the asymmetric setup compared to the symmetric one whereas the temporal deviation decreased with the asymmetric setup. In addition, those differences increased with heat load. This may affect the sensation with thermal environment.
- Further studies are recommended on advanced ventilation methods and heat load layouts to recognize dependencies, regularities and relationships while improving well-being indoors.
- The range of maximum draught rates increased with the asymmetric setup compared to the symmetric one. In the symmetric setup, the local draught rate exceeded 10% at least in one height at all the measured locations and heat load strengths in the occupied zone. In the asymmetric setup, 47% of measured locations exceeded 10% at 40 W/floor-m^2 and 87% at 80 W/floor-m^2, correspondingly. This means that increased heat load, and as a consequence, increased ventilation rate will have a significant effect on the draught discomfort in the occupied zone, although the model may overestimate the draught rate at the arms and feet level.

- The experiments reveal that the average of mean air speeds, the spatial deviation of mean air speeds and the temporal deviation of instantaneous air speeds increased with heat load in both the symmetric and asymmetric setups. Consequently, also the range and maximum of air speeds increased.

Acknowledgement

The authors wish to acknowledge The Foundation LVY sr and The Confederation of Finnish Construction Industries RT for financial support, Professor Arsen Melikov from the Technical University of Denmark and Professor Mats Sandberg from the University of Gävle, Sweden for discussion and comments. The authors would also like to express gratitude to Mr. Etienne Daviet from the Institute National des Sciences Appliquées in Lyon, France, for contributing to the measurements of asymmetric heat load distribution and Doctoral Candidate Weixin Zhao from the Aalto University for contributing to the measurements of air change efficiency.

References

ASHRAE. 2017. *ANSI/ASHRAE Standard 55-2017, Thermal Environmental Conditions for Human Occupancy*. Atlanta: American Society of Heating, Refrigerating and Air-conditioning Engineers, Inc.

Bertheussen, B., P. Mustakallio, R. Kosonen, and A.K. Melikov. 2013. Comparison of the Performance of Chilled Beam with Swirl Jet and Diffuse Ceiling Air Supply: Impact of Heat Load Distribution. *In Proceedings of CLIMA, Prague, Czech Republic, 16-19 June 2013*. Paper ID: 29.

Cao, G., H. Awbi, R. Yao, Y. Fan, K. Sirén, R. Kosonen, and J.J. Zhang. 2014. A review of the performance of different ventilation and airflow distribution systems in buildings. *Building and Environment*, 73:171-186.

Cao, S.J., and H.Y. Deng. 2019. Investigation of temperature regulation effects on indoor thermal comfort, air quality and energy savings towards green residential buildings. Science and Technology for the Built Environment, (Published online) 1-30.

Carrer, P., E. de Oliveira Fernandes, H. Santos, O. Hänninen, S. Kephalopoulos, and P. Wargocki. 2018. On the Development of Health-Based Ventilation Guidelines: Principles and Framework. *Int. J. Environ. Res. Public Health* 2018, 15, 1360.

CEN. 2007. European Standard EN 15251:2007. *Indoor environmental input parameters for design and assessment of energy performance of buildings addressing indoor air quality, thermal environment, lighting and acoustics.* CEN, Brussels, Belgium.

CEN. 2001. European Standard EN ISO 7726:2001. *Ergonomics of the thermal environment. Instruments for measuring physical quantities.* CEN, Brussels, Belgium.

CEN. 2005. European Standard EN ISO 7730:2005. *Ergonomics of the thermal environment — Analytical determination and interpretation of thermal comfort using calculation of the PMV and PPD indices and local thermal comfort criteria.* CEN, Brussels, Belgium.

Cheong, K.W.D., W.J. Yu, S.C. Sekhar, K.W. Tham, and R. Kosonen. 2007. Local thermal sensation and comfort study in a field environment chamber served by displacement ventilation system in the tropics. *Building and Environment*, 42(2), 525-533.

Cho, Y., and H.B. Awbi. 2007. A study of the effect of heat source location in a ventilated room using multiple regression analysis. *Building and environment*, 42(5), 2072-2082.

Fan, J., C.A. Hviid, and H. Yang. 2013. Performance analysis of a new design of office diffuse ceiling ventilation system. *Energy and Buildings*, 59:73-81.

Fanger, P.O. 1970. *Thermal comfort. Analysis and applications in environmental engineering*. Danish Technical Press, Copenhagen, Denmark, ISBN 87 571 0341 0.

Fanger, P.O., A.K. Melikov, H. Hanzawa, and J. Ring. 1988. Air turbulence and sensation of draught. *Energy and buildings*, 12(1):21-39.

Fanger, P.O., and C. Pedersen. 1977. Discomfort due to air velocities in spaces. Proceedings of the Meeting of Commission B1, B2, E1 of the International Institute of Refrigeration, Vol. 4, pp.289-296.

Finkelstein, W., A. Melikov, T. Sefker, and G. Langkilde. 1996. Laser Doppler measurements of airflow characteristics in rooms with mechanical ventilation. Proceedings of Indoor Air'96. Nagoya. Japan. Vol. 1, pp.785-790.

Hagström, K. (2002). Influence of kinetic energy sources and internal obstructions on room air conditioning strategy, efficiency of ventilation and room velocity conditions. Helsinki University of Technology, Department of Mechanical Engineering, Laboratory of Heating, Ventilating and Air Conditioning, ISBN 951-22-6088-3.

Hagström, K., E. Sandberg, H. Koskela, and T. Hautalampi. 2000. Classification for the room air conditioning strategies. *Building and environment*, 35(8):699-707.

Hanzawa, H., A.K. Melikov, and P.O. Fanger. 1987. Airflow characteristics in the occupied zone of ventilated spaces. *ASHRAE Transactions*, 93(1):524-539.

Heiselberg, P. 1994. Draught risk from cold vertical surfaces. *Building and Environment*, 29(3), 297-301.

Heiselberg, P., and P.V. Nielsen. 1996. Flow Element Models. Aalborg: Dept. of Building Technology and Structural Engineering. (Indoor Evironmental Technology; No. 65, Vol. R9657).

Hviid, C.A. and S. Svendsen. 2013. Experimental study of perforated suspended ceilings as diffuse ventilation air inlets. *Energy and Buildings*, 56:160-168.

Jacobs, P., and B. Knoll. 2009. Diffuse ceiling ventilation for fresh classrooms. *In Proceedings of 30th AIVC Conference "Trends in High Performance Buildings and the Role of Ventilation", Berlin, Germany, 1-2 October 2009*.

Jacobs, P., E.C. van Oeffelen, and B. Knoll. 2008. Diffuse ceiling ventilation, a new concept for healthy and productive classrooms. *In Proceedings of Indoor Air, Copenhagen, Denmark, 17-22 August 2008*. Paper ID: 3.

Kandzia, C., and D. Müller. 2016. Flow structures and Reynolds number effects in a simplified ventilated room experiment. International Journal of Ventilation, 15(1), 31-44.

Karmann, C., S. Schiavon, and F. Bauman. 2017. Thermal comfort in buildings using radiant vs. all-air systems: A critical literature review. *Building and Environment*, 111:123-131.

Koskela, H., H. Häggblom, R. Kosonen, and M. Ruponen. 2010. Air distribution in office environment with asymmetric workstation layout using chilled beams. *Building and Environment*, 45(9), 1923-1931.

Koskela, H., H. Häggblom, R. Kosonen, and M. Ruponen. 2012. Flow pattern and thermal comfort in office environment with active chilled beams. *HVAC&R Research*, 18(4):723-736.

Kosonen, R., M. Ahola, K. Villberg, and T. Takki. 2011. Perceived IEQ conditions: why the actual percentage of dissatisfied persons is higher than standards indicate? In: Abdul-Wahab SA (ed): *Sick Building Syndrome*. Springer Berlin Heidelberg, pp. 75–88.

Kosonen, R., P. Saarinen, H. Koskela, and A. Hole. 2010. Impact of heat load location and strength on air flow pattern with a passive chilled beam system. *Energy and Buildings*, 42(1), 34-42.

Lan, L., P. Wargocki, D.P. Wyon, and Z. Lian. 2011. Effects of thermal discomfort in an office on perceived air quality, SBS symptoms, physiological responses, and human performance. *Indoor Air*, 21(5):376-390.

Larsson, U., and B. Moshfegh. 2002. Experimental investigation of downdraught from well-insulated windows. *Building and Environment*, 37(11):1073-1082.

Lestinen, S., S. Kilpeläinen, R. Kosonen, J. Jokisalo, and H. Koskela. 2018b. Experimental study on airflow characteristics with asymmetric heat load distribution and low-momentum diffuse ceiling ventilation. *Building and Environment*, 134:168-180.

Lestinen, S., S. Kilpeläinen, R. Kosonen, J. Jokisalo, H. Koskela, and A. Melikov. 2018a. Flow characteristics in occupied zone – An experimental study with symmetricly located thermal plumes and low-momentum diffuse ceiling air distribution. *Building and Environment*, 128:77–88.

Liu, S., S. Schiavon, A. Kabanshi, and W.W. Nazaroff. 2017. Predicted percentage dissatisfied with ankle draft. *Indoor Air*, 27(4):852-862.

Mayer, E., and R. Schwab. 1988. Direction of low turbulent airflow and thermal comfort. *In Proceedings of Healthy Buildings 88, Stockholm, Sweden, Vol.2*.

Melikov, A.K. 2004. Personalized ventilation. *Indoor Air*, 14:157-167.

Melikov, A.K., H. Hanzawa, and P.O. Fanger. 1988. Airflow characteristics in the occupied zone of heated spaces without mechanical ventilation. *ASHRAE Transactions*, 94(1):52-70.

Melikov, A.K., U. Krüger, G. Zhou, T.L. Madsen, and G. Langkilde. 1997. Air temperature fluctuations in rooms. *Building and Environment*, 32(2), 101-114.

Melikov, A., G. Pitchurov, K. Naydenov, and G. Langkilde. 2005. Field study on occupant comfort and the office thermal environment in rooms with displacement ventilation. Indoor air, 15(3), 205-214.

Melikov A.K., Z. Popiolek, M.C.G. Silva, I. Care, and T. Sefker. 2007. Accuracy limitations for low-velocity measurements and draft assessment in rooms. *HVAC&R Research*, 13(6):971-986.

Müller, D., C. Kandzia, R. Kosonen, A.K. Melikov, and P.V. Nielsen. 2013. *Mixing Ventilation. Guide on mixing air distribution design*. Federation of European Heating and Air-Conditioning Associations, REHVA, ISBN 978-2-930521-11-4.

Mustakallio, P., Z. Bolashikov, K. Kostov, A. Melikov, and R. Kosonen. 2016. Thermal environment in simulated offices with convective and radiant cooling systems under cooling (summer) mode of operation. *Building and Environment*, 100:82-91.

Mustakallio, P., Z. Bolashikov, L. Rezgals, A. Lipczynska, A. Melikov, and R. Kosonen. 2017. Thermal environment in a simulated double office room with convective and radiant cooling systems. *Building and Environment*, 123:88-100.

Nielsen, P.V. 2007. Analysis and design of room air distribution systems. *HVAC&R Research*, 13(6), 987-997

Nielsen, P.V. 2011. The "Family Tree" of Air Distribution Systems. *In Proceedings of Roomvent, Trondheim, Norway, 19-22 June 2011*. Paper No: 316.

Nielsen, P.V., R.W. Vilsbøll, L. Liu, and R.L. Jensen. 2017. Diffuse Ceiling Ventilation, Load Distribution and Ceiling Design. *In Proceedings of Healthy Buildings Europe, Lublin, Poland, July 2-5 2017*. Paper ID 0026.

Olesen, B.W. 2000. Guidelines for comfort. *Ashrae Journal*, 42(8), 41.

Petersen, S., N.U. Christensen, C. Heinsen, and A.S. Hansen. 2014. Investigation of the displacement effect of a diffuse ceiling ventilation system. *Energy and Buildings*, 85, 265-274.

Sakellaris, I. A., D.E. Saraga, C. Mandin, C. Roda, S. Fossati, Y. de Kluizenaar, ... and O. Hänninen. 2016. Perceived indoor environment and occupants' comfort in European "modern" office buildings: the OFFICAIR study. *International journal of environmental research and public health*, 13(5):444.

Seppänen, O.A., W.J. Fisk, and M.J. Mendell. 1999. Association of ventilation rates and CO2 concentrations with health and other responses in commercial and institutional buildings. *Indoor air*, 9(4):226-252.

Seppänen, O.A., and W.J. Fisk. 2004. Summary of human responses to ventilation. *Indoor Air*, 14:102-118.

Shao, X., K. Wang, X. Li, and Z. Lin. 2018. Potential of stratum ventilation to satisfy differentiated comfort requirements in multi-occupied zones. *Building and Environment*, 143, 329-338.

Toftum, J. 2004. Air movement–good or bad?. *Indoor Air*, 14:40-45.

Toftum, J., G. Zhou, and A. Melikov. 1997. Effect of airflow direction on human perception of draught. *In Proceedings of CLIMA 2000, Aug.30-Sept.2 1997, Brussels*. Paper 366.

Wargocki, P., J. Sundell, W. Bischof, G. Brundrett, P.O. Fanger, F. Gyntelberg, S.O. Hanssen, P. Harrison, A. Pickering, O. Seppänen, and P. Wouters. 2002. Ventilation and health in non-industrial indoor environments: report from a European Multidisciplinary Scientific Consensus Meeting (EUROVEN). *Indoor air*, 12(2), 113-128.

Wargocki, P., and D.P. Wyon. 2007. The effects of moderately raised classroom temperatures and classroom ventilation rate on the performance of schoolwork by children (RP-1257). Hvac&R Research, 13(2), 193-220.

Wierzbicka, A., E. Pedersen, R. Persson, B. Nordquist, K. Stålne, C. Gao, L. E. Harderup, J. Borell, H. Caltenco, B. Ness, E. Stroh, Y. Li, M. Dahlblom, K. Lundgren-Kownacki, C. Isaxon, A. Gudmundsson, and P. Wargocki. 2018. Healthy Indoor Environments: The Need for a Holistic Approach. *International journal of environmental research and public health*, 15(9), 1874.

Yin, S., Y. Li, Y. Fan, and M. Sandberg. 2019. Experimental investigation of near-field stream-wise flow development and spatial structure in triple buoyant plumes. *Building and Environment*, 149, 79-89.

Zhang, C., P. Heiselberg, and P.V. Nielsen. 2014. Diffuse Ceiling Ventilation-A Review. *International Journal of Ventilation*, 13(1), 49-63.

Zhang, C., M.H. Kristensen, J.S. Jensen, P.K. Heiselberg, R.L. Jensen, and M. Pomianowski. 2016. Parametrical analysis on the diffuse ceiling ventilation by experimental and numerical studies. *Energy and Buildings*, 111, 87-97.

Zukowska-Tejsen, D., M. Wolsing, M. Grysbæk, and C.A. Hviid. 2016. Field Study of Diffuse Ceiling Ventilation Performance in a Landscape Office. *In CLIMA 2016 - proceedings of the 12th REHVA World Congress (ed PK Heiselberg), Aalborg, Denmark, 22-25 May 2016*. Paper No: 478.